PREPRINT SUBMITTED

This manuscript is a preprint uploaded to EarthArXiv, not yet peer-reviewed. This preprint is submitted for publication to *Geochemistry, Geophysics, Geosystems* in March 2024. Authors encourage downloading the latest manuscript version from EarthArXiv, and welcome comments, feedback and discussions anytime. Please, feel free to get in contact with the first author: gino@ginodegelder.nl

Reconstructing Quaternary sea-level through bayesian inversion of staircase coastal landscapes

Gino de Gelder[1,2,3*], Navid Hedjazian[3], Laurent Husson[1], Thomas Bodin[3], Anne-Morwenn Pastier[4], Yannick Boucharat[1], Kevin Pedoja[5], Tubagus Solihuddin[2], Sri Yudawati Cahyarini[2]

1) ISTerre, IRD, CNRS, Université Grenoble-Alpes, France
2) Res. Group for Paleoclimate and Paleoenvironment, Research Center for Climate and Atmosphere, BRIN, Bandung, Indonesia
3) CNRS, LGL-TPE, Universite Claude Bernard Lyon1, ENS de Lyon, France
4) GFZ Potsdam, Germany
5) Université de Caen Normandie

**Corresponding author: gino@ginodegelder.nl*

Reconstructing sea-level and hydroclimates through Bayesian inversion of coastal landforms

G. de Gelder[1,2,3], N. Hedjazian[3], L. Husson[1], T. Bodin[3], A.-M. Pastier[4], Y. Boucharat[1], K. Pedoja[5], T. Solihuddin[2] and S. Y. Cahyarini[2]

[1]ISTerre, IRD, CNRS, Université Grenoble-Alpes, France

[2]Res. Group of Paleoclimate & Paleoenvironment, Res. Centr. for Climate and Atmosphere, Res. Org. of Earth Sciences and Maritime, National Research and Innovation Agency, Bandung, Republic of Indonesia.

[3]CNRS, LGL-TPE, Universite Claude Bernard Lyon1, ENS de Lyon, France

[4]GeoForschungsZentrum, Potsdam, Germany

[5]Université de Caen, Caen, France

Corresponding author: Gino de Gelder (gino.de-gelder@univ-grenoble-alpes.fr)

Key Points:

- We developed a methodology to invert marine terrace sequences and simultaneously obtain sea-level, uplift rate and other constraints
- Parameter ranges are better constrained for faster uplifting sequences, and for joint inversion of multiple profiles
- We solve paleo-sea/lake level for the Gulf of Corinth, proposing marine, transitional, overfilled lake and underfilled lake stages

Abstract

Quantifying Quaternary sea-level changes and hydroclimatic conditions is an important challenge given their intricate relation with paleo-climate, ice-sheets and geodynamics. The world's coastlines provide an enormous geomorphologic archive, from which forward landscape evolution modelling studies have shown their potential to unravel paleo sea-levels, albeit at the cost of assumptions to the genesis of these landforms. We take a next step, by applying a Bayesian approach to jointly invert the geometries of multiple coastal terrace sequences to paleo sea- and lake level variations and extract past hydroclimatic conditions. Using a Markov chain Monte Carlo sampling method, we first test our approach on synthetic marine terrace profiles as proof of concept and benchmark our model on an observed marine terrace sequence in Santa Cruz (US). We successfully reproduce observed sequence morphologies and simultaneously obtain probabilistic estimates for past sea-level variations, as well as for other model parameters such as uplift and erosion rates. When applied to the semi-isolated Gulf of Corinth (Greece), our method allows to decipher the geomorphic Rosetta stone at an unprecedented resolution, revealing the connectivity between the Lake/Gulf of Corinth and the open sea for different hydroclimatic conditions. Eustatic sea-level and changing sill depths drive marine and transitional phases during interglacial and interstadial periods, whereas wetter and drier hydroclimates respectively over- and under-fill Lake Corinth during interstadial and glacial periods.

1 Introduction

Reconstructions of Quaternary sea-level variations provide crucial constraints on thresholds and feedbacks within climatic and geodynamic systems that help understand how contemporary climate change may affect future sea level (Lambeck and Chappell, 2001; Hay et al., 2014; Dutton et al., 2015; Shakun et al,. 2015; Austermann et al,. 2017). A key archive of past sea-level is exposed within the geomorphology of most of the world's coastal areas in the form of paleo-shorelines (Johnson and Libbey, 1997; Pedoja et al., 2011, 2014; Rovere et al., 2023; Fig. 1a), but it remains difficult to accurately translate coastal observations and measurements into paleo-sea-level estimates, and to evaluate the uncertainties inherent to these conversions. Major challenges include 1) the dating of these landforms, as most paleo-shorelines are erosive in nature (Pedoja et al., 2014) and absolute dating techniques themselves are complex and prone to large uncertainties (Strobl et al., 2014; Hibbert et al., 2016; Ott et al., 2019), 2) the bias of observations, which are mostly restricted to the most recent glacial cycle(s) and to periods where relative sea level was at similar elevations to present-day (Medina-Elizalde, 2013; Hibbert et al., 2016), 3) the absence of reciprocity between paleo-shorelines and sea-level stands, as not all highstands lead to paleo-shorelines, and paleo-shorelines may have formed during one or many sea-level cycles (Guilcher, 1974; Malatesta et al., 2021; Chauveau et al., 2023), and 4) separating the tectonic from the sea-level component within relative sea-level changes (Pedoja et al., 2011).

Numerical models of landscape evolution started to overcome some of these limitations, by providing a means to quantitatively interpret undated paleo-shorelines, incorporate full sea-level curves instead of highstands only, unravelling the creation of paleo-shorelines formed over multiple glacial cycles, and considering multiple sea-level curves (e.g. Webster et al., 2007; Jara-Muñoz et al., 2019; Leclerc and Feuillet, 2019; De Gelder et al., 2020; 2023). So far, such numerical models have mainly been used for forward modelling approaches, where a number of proposed sea-level curves are used to predict shorelines, which are then compared to actual observations. However, this only provides a limited way to explore the full ensemble of possible sea-level histories and other model parameters like rock erosion rates or effective wave base depths, which are difficult to estimate. It follows that uncertainties in sea-level estimates from marine terraces remain poorly known, regardless of the method used, and in spite of uniformization attempts (Lorscheid and Rovere, 2019).

A hydrodynamic setting for which it is particularly complex to reconstruct sea-level is that of semi-isolated marine basins, i.e. bodies of water that have been connected to the open sea in some intervals of their geologic history, and little or disconnected from the sea in other intervals. Such settings, like the Red Sea, Sea of Marmara (Turkey), Carioco Basin (Venezuela) and Gulf of Corinth (Greece), have a special geologic interest, given the active tectono-sedimentary processes driving their formation (e.g. Van Daele et al., 2011; McNeill et al., 2019), their sensitivity to rapid sea-level and climatic changes (e.g. Aksu et al., 1999; Siddall et al., 2004), and their role in dispersion of species (e.g. Derricourt, 2005). The main complexity in reconstructing sea-/lake-level fluctuations in such settings, is that 1) during disconnected phases these basins may have been underfilled or overfilled depending on local hydroclimate, and 2) the structural highs (sills) separating the basins from the sea can be simultaneously affected by tectonic vertical motion, sedimentation and erosion.

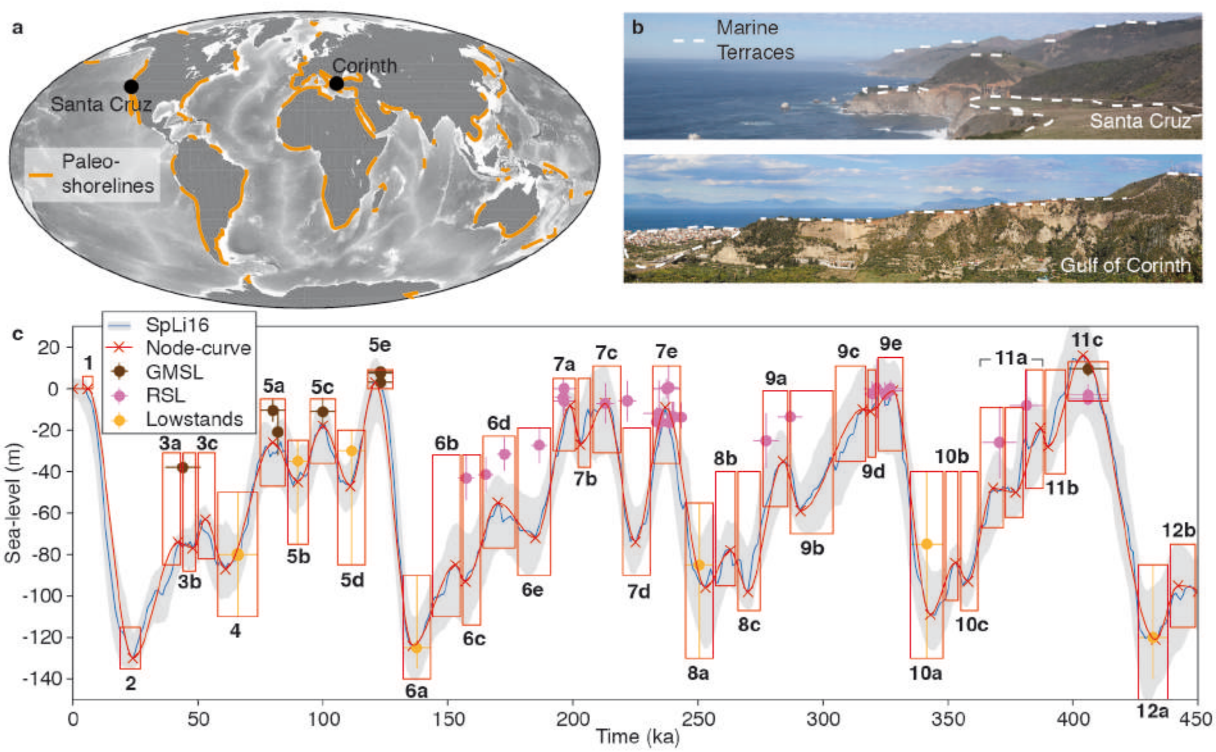

Figure 1. Paleo-shorelines and paleo-sea level. a) Global compilation of paleoshoreline sequences, adjusted from Pedoja et al., 2014, **b)** pictures of marine terrace sequences from Santa Cruz (US) and the Corinth Rift (Greece) and **c)** paleo-sea-level estimates for the past 450 ka, showing a sea-level curve (SpLi16, blue; Spratt and Lisiecki, 2016) derived from principal component analysis of 7 sea-level curves with its 2.5% and 97.5% likelihood range (grey envelope), an approximation of that curve with nodes and a cubic spline interpolation (red),

global mean sea-level highstand estimates adjusted for glacio-istostatic adjustments (GMSL, brown; Kopp et al., 2009; Dutton et al., 2015; Pico et al., 2016; Creveling et al., 2017; Dyer et al., 2021; Tawil-Morsink et al,. 2022), selected relative sea-level highstand estimates >130 ka (RSL, pink; Stirling et al., 2001; Murray-Wallace, 2002; Andersen et al., 2010 de Gelder et al., 2022; Marra et al., 2023), global mean sea-level lowstand estimates from ice sheet data (orange; Batchelor et al., 2019), and red boxes that represent the likely admissible range of relative sea-level elevations at locations far from the major ice-sheets (details in Supplementary Information) that we consider in this study. Marine Isotope Stages (MIS) are given in bold, and based on Railsback et al., 2015.

In this study, we intend to overcome common marine terrace analysis limitations, by using a Bayesian approach to invert the geometry of paleo-shoreline sequences. Our approach provides probabilistic estimates of paleo sea-level, erosion rates, uplift rates, wave-based depths and initial slopes. We focus on erosive marine terraces (Fig. 1b), which are both the most common type of paleo-shoreline (Pedoja et al., 2014), and are simpler to model than their depositional and bio-constructed equivalents (e.g. Pastier et al., 2019). We first apply our probabilistic inversion approach to a set of synthetic coastal profiles to test and illustrate the method, after which we invert a well-studied marine terrace sequence in Santa Cruz (US) to benchmark our model on a natural example. Finally, we use our approach on the semi-isolated Gulf of Corinth to decipher the complex combination of tectonic uplift, sea- and lake-level fluctuations, local climatic drivers and sill dynamics. These case studies highlight how we can derive probabilistic estimates of past sea-level from marine terraces, and how the natural archive of paleo-shorelines can be further utilized to improve both paleo sea-level estimates, and unravel complex tectono-hydro-climatic interactions.

2 Marine terrace sequence inversion

In Marine terraces are relatively flat surfaces of coastal origin, either horizontal or gently inclined seawards (Fig 1b; Pirazzoli, 2005). They are bounded inland by a fossil sea-cliff, and can be covered by a layer of coastal sediments. Here we model erosive marine terraces, which are primarily formed by sea-cliff retreat in response to wave action. The superposition of Quaternary sea-level variations (Fig. 1c) and vertical land movement typically leads to a staircase landscape exhibiting marine terraces sequences (Fig. 1b; Lajoie, 1986).

The landscape evolution model we use (REEF; Husson et al., 2018; Pastier et al., 2019) has a wave erosion module based on the wave energy dissipation model developed by Anderson et al. (1999). The model assumes that the vertical seabed erosion rate is a linear function of the rate of wave energy dissipation against the seabed (Sunamura, 1992). Horizontal erosion rates depend on the energy available at the sea-cliff after dissipation of the far-field wave energy (Anderson et al., 1999). The dissipation rate is dictated by the water depth profile, which increases landwards exponentially with decreasing water depth. The 2D model we use consists of a landmass with a sea-ward dipping linear initial slope (IS; Fig. 2a), an initial erosion rate (ER; Fig. 2a) that evolves as platforms are being carved, a wave base depth (WB; Fig. 2a) that determines the vertical range over which erosion takes place, a land uplift rate (UR; Fig. 2a) and a sea-level history. Equations and detailed descriptions can be found in Anderson et al. (1999) and Pastier et al. (2019).

To invert the morphology of the marine terrace sequences, we parameterize the sea-level history with a finite number of unknown parameters. We use nodes interpolated through a cubic spline scheme (Fig. 2b; light blue). This creates sea-level curves with similar characteristics to published sea-level curves (red line, Fig. 1c), in which the nodes represent sea-level minima (lowstands) and maxima (highstands) that are typically linked to even and odd-numbered marine isotope stages (MIS), respectively. In the Monte Carlo exploration of the model space, nodes can either be fixed at certain ages and elevations, or left free to move within a prescribed range (e.g. red boxes in Fig. 2b,d,e). The 4 main erosion model parameters (IS, ER, WB, UR) can also be fixed to chosen values, as done in the synthetic tests below, or left free within chosen ranges, as done for the Santa Cruz and Corinth examples below.

In a Bayesian framework, the solution is a posterior probability distribution describing the probability of the model parameters (here the past sea-level variations), given the observed data (here the geometry of marine terraces). We use a Markov chain Monte Carlo algorithm to sample the posterior distribution and explore the range of models that can explain the observed topography within errors. The solution is a large ensemble of paleo sea-level models that approximates the probabilistic solution. That is, the distribution of models follows the posterior probability solution. For a review of Bayesian inference and Monte Carlo methods in the geosciences, we refer the reader to Mosegaard and Sambridge (2002), and Gallagher et al. (2009).

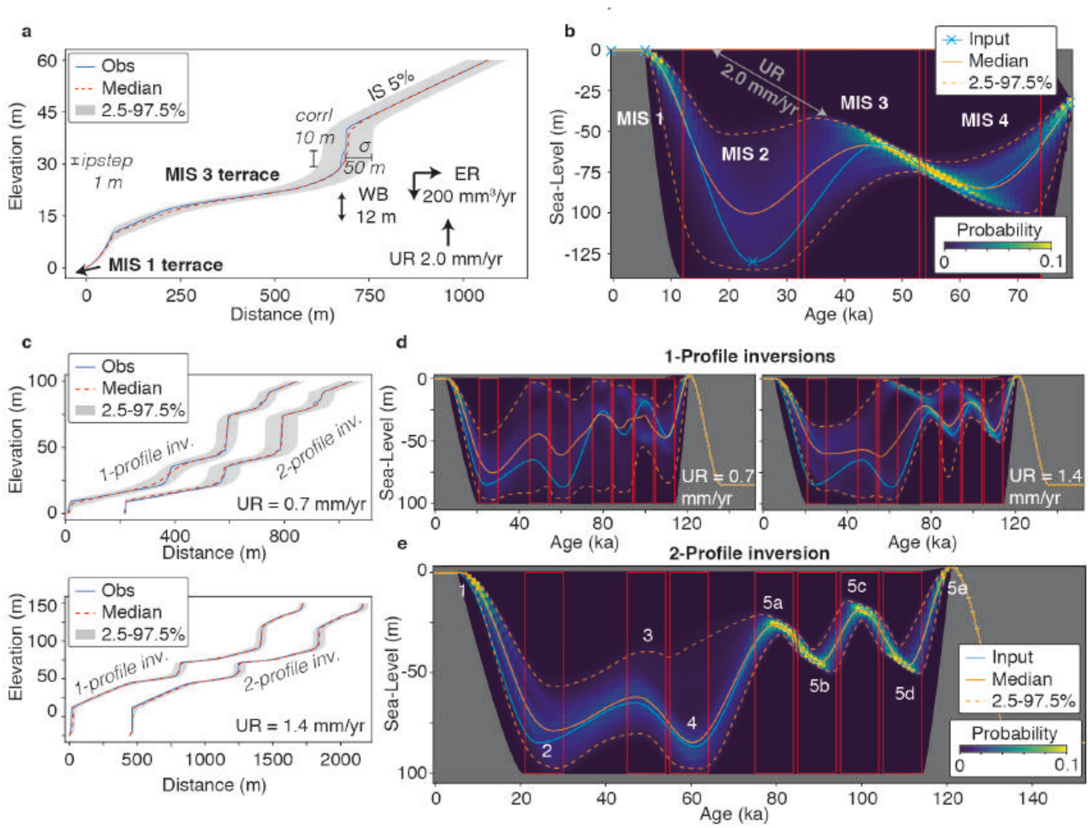

Figure 2. Inversion of synthetic marine terrace profiles. a) Synthetic topography (Obs, blue) created from a forward model with known input parameters: IS = Initial Slope, ER = Erosion Rate, UR = Uplift Rate and WB = Wave Base. The range of inverted models that fit the observed topography with the given σ, ipstep and corrl (see text) is represented by the median (orange), and the 2.5 and 97.5 percentiles of the inverted models (grey envelope). **b)** Posterior probability distribution for the sea-level histories. Each individual paleo sea-level history is described with 6

sea-level nodes linked with a cubic spline interpolation, of which the nodes at 78, 6 and 0 ka are fixed in time and elevation, and the other three nodes can move within the three red boxes. The input (target) sea-level history is given in light blue, and the probabilistic solution is depicted by the median (solid orange line) and the 2.5 and 97.5 percentiles (dashed orange lines). **c)** Same as **a**, but with different uplift rates and sea-level histories. **d)** Sea-level histories for the inverted profiles in **c**, similar to **b** but with a different input sea-level history including more nodes. **e**) Similar to **d**, but inverting the two profiles simultaneously to find a common sea-level curve explaining both profiles. MIS are marked in white.

One benefit of Bayesian inference is the ability to propagate uncertainty estimates from the observed measurements towards the unknown model parameters. For that, a likelihood probability distribution needs to be defined, based on a misfit function and on uncertainty estimates associated to observations. In this work, the data vector is defined as a set of points measured on the shoreline with a vertical step size (ipstep; Fig. 2a). The misfit between this data vector and the modelled paleo-shoreline sequences is calculated on the horizontal axis, as the variability of marine terrace width within a section of coastline is typically much higher than the variability in marine terrace height (e.g. Regard et al., 2017; De Gelder et al., 2020). Uncertainties about the observed shorelines account for the inability of our numerical model to explain observations. These errors are treated as Gaussian random errors and described by a standard deviation (σ; Fig. 2a) and the level of spatial correlation (corrl; Fig 2a).

3 Synthetic marine terrace profiles

To test and illustrate the potential of the inversion approach, we inverted synthetic topographic profiles that were produced by forward models with known input parameters (Fig. 2). To start with a relatively short and simple sea-level range, we defined an 80 ka sea-level history consisting of 6 nodes (Fig. 2b; light blue). For the inversion, we fixed the nodes at 78, 6 and 0 ka, and the positions of the other three nodes were left as unknown model parameters to be recovered. In the Monte Carlo exploration of the model space, these three nodes were left free to move within a prescribed range (red boxes in Fig. 2b). All other erosion model parameters (IS, ER, WB, UR; Fig. 2a) were fixed during the inversion at the values used to produce the observed topographic profile. The parameters σ, ipstep and corrl were set at 50, 1 an 10 m, respectively. We inverted the topographic profile between 0 and 60 m elevation by sampling the parameter space with 1 million forward simulations. The solution is a large ensemble of sea-level histories that reflect the probability of the paleo sea-level, given the synthetic coastline topography.

The resulting profiles show an MIS 3 terrace at an elevation range of ~15-30 m (Fig. 2a), whereas an MIS 1 terrace lies below the present-day sea level, and is thus not considered in the inversion. As such, the range of sea-level histories that could have created the MIS 3 terrace is narrower than for the MIS 1 terrace (Fig. 2b). This range is particularly limited for the period of sea-level rise leading up to the MIS 3 peak, suggesting that uplifted marine terraces are more likely to form during periods of relative sea-level rise. This is theoretically expected, as erosion scales with the total duration of sea-level occupation (Malatesta et al., 2021), and simultaneous sea-level rise and land uplift implies favorable conditions for the formation of marine terraces. Another notable feature is the distribution of possible sea-level histories along a diagonal line that corresponds to the uplift rate. This line would reach the maximum terrace elevation when extrapolated to t=0 ka, in line with classic graphical methods (Bloom and Yonekura, 1990). Although the MIS 1 terrace is not inverted, there are some limitations to the magnitude and rate of sea-level rise between MIS 2 and MIS 1 (Fig. 2b), probably because this period determines how much of the MIS 3 terrace is eroded at its distal edge.

For the inversion of every individual profile there should be a trade-off between younger, higher sea-level peaks and older, lower sea-level peaks in line with the fixed uplift rate (as in Fig. 2b). These trade-off effects can be overcome through the joint inversion of multiple profiles with different uplift rates, reducing the uncertainty in sea-level reconstructions. To show this, we also inverted two different topographic profiles produced with different fixed uplift rates but with the same sea-level history over a 135 ka timescale (the last glacial-interglacial cycle; Fig. 2c-e). When the two profiles are inverted individually, the range of possible sea-level histories is relatively wide, and again the sea-level peaks would follow a diagonal line parallel to the uplift rate (Fig. 2c, d). However, if we jointly invert both profiles, i.e. assuming that a unique sea-level history would have created both marine terrace staircase morphologies, the probability distribution for past sea-level narrows, and the median sea-level of the inversion better approximates the input curve (Fig. 2e). The range is particularly narrow for the transgressions leading up to the MIS 5a and 5c highstands, for which the corresponding terraces are well developed in the topographic profiles (Fig. 2c). Similar to the MIS 1 terrace in Fig. 2a, the MIS 1 and 3 terraces in Fig. 2c would be located below sea level for the given parameters, and thus the possible sea-level range is wider for the transgressions leading up to MIS 1 and 3 (Fig. 2d). Also for these highstands though, the sea-level is better constrained for the joint inversion (Fig. 2e) than with the individual inversions (Fig. 2d). This suggests that jointly inverting more profiles would increase even further our ability to constrain sea-level histories.

These synthetic tests imply that in natural examples, sea-level reconstruction should also benefit from the inversion of multiple marine terrace profiles if conditions change between those profiles. In this example we used two different uplift rates for the joint inversion, which lead to a range in different terrace sequence morphologies (Fig. 2c), but an approach where all parameters, including wave base, erosion rate or initial slope, are undefined *a priori* (or only within a given range), should lead to a more realistic range of possible sea-level histories. To put this method to the test in real cases, we selected two well-documented yet contrasting cases, Santa Cruz and the Gulf of Corinth, each having their peculiarities that make them ideal to study the inversion of marine terraces.

4 Santa Cruz marine terrace sequence inversion

The marine terraces along the Santa Cruz coastline (central California, US) formed through a combination of Quaternary sea-level oscillations and tectonic uplift by nearby active faults (e.g. Bradley, 1957; Anderson and Menking, 1994; Anderson et al., 1999; Perg et al., 2001; Matsumoto et al., 2022). We invert a topographic profile from Rosenbloom and Anderson (1994), who distinguished the original eroded bedrock surface, which we use, from its overlying colluvium for 5 marine terraces. We followed the age interpretation of Perg et al. (2001), suggesting these terraces were formed, from bottom to top, during MIS 1, 3, 5a, 5c and 5e. Unlike in the synthetic tests, here we left the uplift rate, erosion rate, wave base depth and initial slope parameters free within a range of values. We use the elevation (~170 m) and age of the upper terrace to derive a range of possible uplift rates (1.3-1.65 mm/yr), and simultaneously consider ranges for initial slope (5-15%), wave base depth (1-10 m) and erosion rates (100-800 mm^3/yr) in the terrace inversion. We use the same inversion parameters as for the synthetic tests, running 1 million models over 450 ka with the sea-level high- and lowstands limited to the red boxes in Fig. 1 (See Supplementary Information). Tests with different inversion parameters are given in Fig. S1, but these do not change the paleo sea-level estimates much.

The sampled sea-level histories successfully reproduce the terrace morphology, as evidenced by the low RMS misfit of 2 m (Fig. 3a). As with the synthetic tests (Fig. 2), periods of sea-level rise are better constrained than periods of sea-level fall, and highstands better constrained than lowstands (Fig. 3b). Also here there is a trade-off in sea-level peaks, in which younger, higher sea-level peaks could result in similar shaped marine terraces as older, lower sea-level peaks (e.g. for MIS 3c, Fig. 3e). The models limit the uplift rate to ~1.35-1.6 mm/yr, the initial slope to ~7-9.5%, the wave base depth to 4-10 m and the erosion rate to 200-800 mm/yr (Figs. 3c,d). Notably there is a positive correlation between wave base depth and erosion rate (Fig. 3d), suggesting a higher value for wave base depth would require a higher erosion rate to create the same marine terrace sequence morphology.

Compared to our proposed range of possible sea-level elevations for MIS 3 (-30 to -80 m; Fig. 3b), the inversion suggests paleo sea-level values on the higher end of that spectrum. This is in agreement with a growing number of studies suggesting oxygen-isotope derived sea-level curves underestimate sea-level for that period (Pico et al., 2016; Dalton et al., 2019, 2022; Gowan et al., 2021; De Gelder et al., 2022). For MIS 5a on the other hand, the inversion suggests a sea-level peak on the lower end of our proposed range of sea-level elevations (Fig. 3b). Although the highstand solutions still span a broad elevation range of ~25 m, the inversion results tend to align with studies proposing an overall decrease in sea-level between MIS 5e, 5c and 5a (e.g. Chappell and Shackleton, 1986; Schellmann & Radtke, 2004; Tawil-Morsink et al., 2022).

We also tested additional uplift rate scenarios (Fig. S2), given that there has been concerns on the terrace chronology that we adopted (Brown and Bourlès, 2002), and other studies have suggested the terrace at 27 m elevation might be formed during MIS 5a, 5c or 5e instead of MIS 3 (Bradley and Addicott, 1968; Lajoie et al., 1975; Kennedy et al., 1982; Weber et al., 1990). These uplift rates can fit the terrace sequence morphology equally well in terms of topographic misfit, but generally imply a larger possible range of paleo sea level. This can be explained by the increased terrace re-occupation for lower uplift rates (Malatesta et al., 2021), which also explains why the possible ranges for the initial slope and wave base depth change increase for lower uplift rate scenarios (Fig. S2), and erosion rate estimates decrease. These tests suggest that locations with higher uplift rates will generally provide narrower constraints on paleo sea-level, while still providing realistic and unbiased parameter estimates.

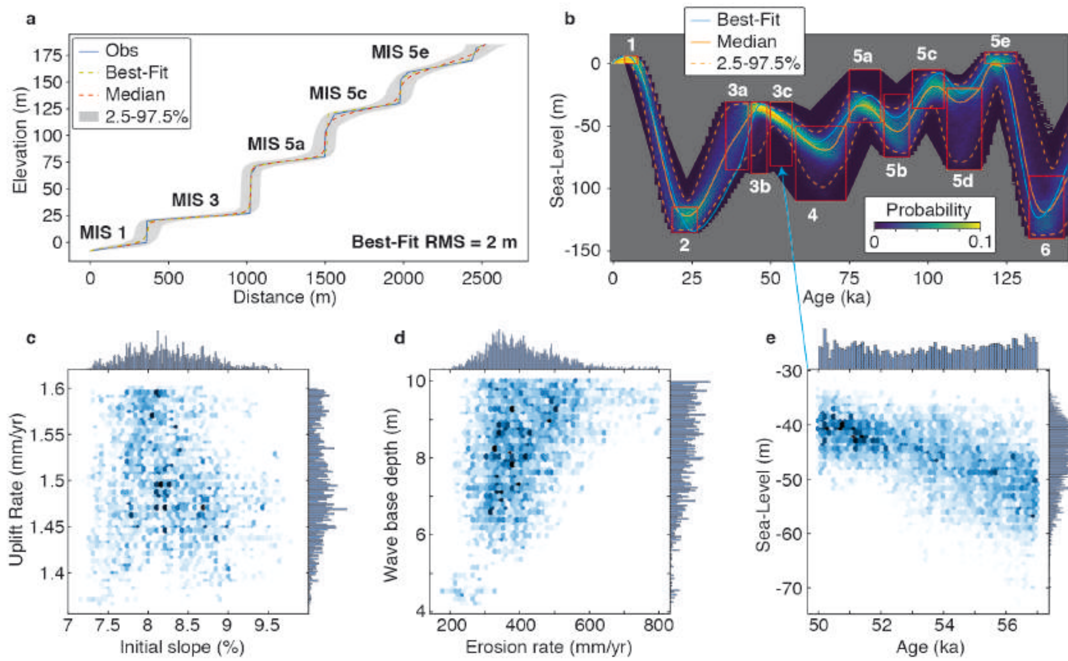

Figure 3. Inversion of NW-Santa Cruz marine terrace sequence. a) Observed topography (from Rosenbloom and Anderson, 1994; Obs, blue) with the age interpretation of Perg et al. (2001) marked in bold, together with the modeled best-fit, median, 2.5% and 97.5% percentile profiles. **b)** Probabilistic sea-level reconstruction for the profiles in **a**, MIS in white **c)** Probabilistic solution for uplift rates and initial slopes (histogram of the sampled models), **d)** Probabilistic solution for wave base depths and erosion rates **e)** 2D marginal probabilistic solution for the MIS 3c peak, i.e. distribution for the position of the 50-57 ka node within the paleo sea level curve.

5 Gulf of Corinth marine terrace sequence inversion

The complexity of semi-isolated basins, connected to sea during some time intervals and isolated in others, make them ultimate testing grounds for our modelling approach. We focus on one of such basins, the SE Gulf of Corinth, to derive a sea-/lake-level history from terrace sequence geometries, and compare its outcomes to paleoclimate data, tectonic structures and sill dynamics.

Natural interaction between the Gulf of Corinth and the open sea is currently restricted by the Rion and Acheloos-Cape Pappas sills at its W entrance at ~45-60 m depth (Fig. 4; Beckers et al., 2016). In the past there was an additional connection at its E end along the Corinth Isthmus, currently uplifted at ~80 m elevation but consisting of Quaternary marine sediments (Fig. 4; Caterina et al., 2023). These sills have controlled the Gulf's connection with the open sea over the past few hundred thousand years and lead to an alternation of marine and (semi-)isolated lake environments within the Gulf (McNeill et al., 2019). Although we approximately know the timing of these alternations, it remains unclear whether lake levels were stable or fluctuating during periods with no connection to the sea, and whether sill depths remained stable or fluctuated throughout the Quaternary (Roberts et al., 2009; McNeill et al., 2019).

Terrace sequences are well exposed in the SE of the Gulf, where the Gulf of Corinth Fault System (Fig. 4) has lead to differential coastal uplift rates (Armijo et al., 1996; De Gelder et al., 2019; Fig. S3). This peculiarity allows us to test on a natural example whether the joint inversion of multiple terrace sequence profiles with different uplift rates provides a better-constrained sea-/lake-level history (as in Fig. 2). To account for the unknown range of possible lake-level elevations, we carried out inversions with all nodes from (semi-)isolated periods broadly constrained between -15 and -150 m elevation. We selected three topographic profiles with little river incision and ~0.4-1.45 mm/yr uplift rates (Fig. S3), and avoided modelling the broad coastal plains at the base of all profiles that appear to have been modified by human presence (Fig. S3). We used the 90% percentile of 100-m wide swath profiles to obtain representative terrace sequence morphologies (Fig. S3). For the three profiles we assigned ranges of possible uplift rates of 1.25-1.4, 0.7-0.9 and 0.4-0.55 mm/yr (De Gelder et al., 2019; Fig. S3), and broad ranges for erosion rate (100-1500 mm/yr), initial slope (1-20%) and wave base depth (1-12 m).

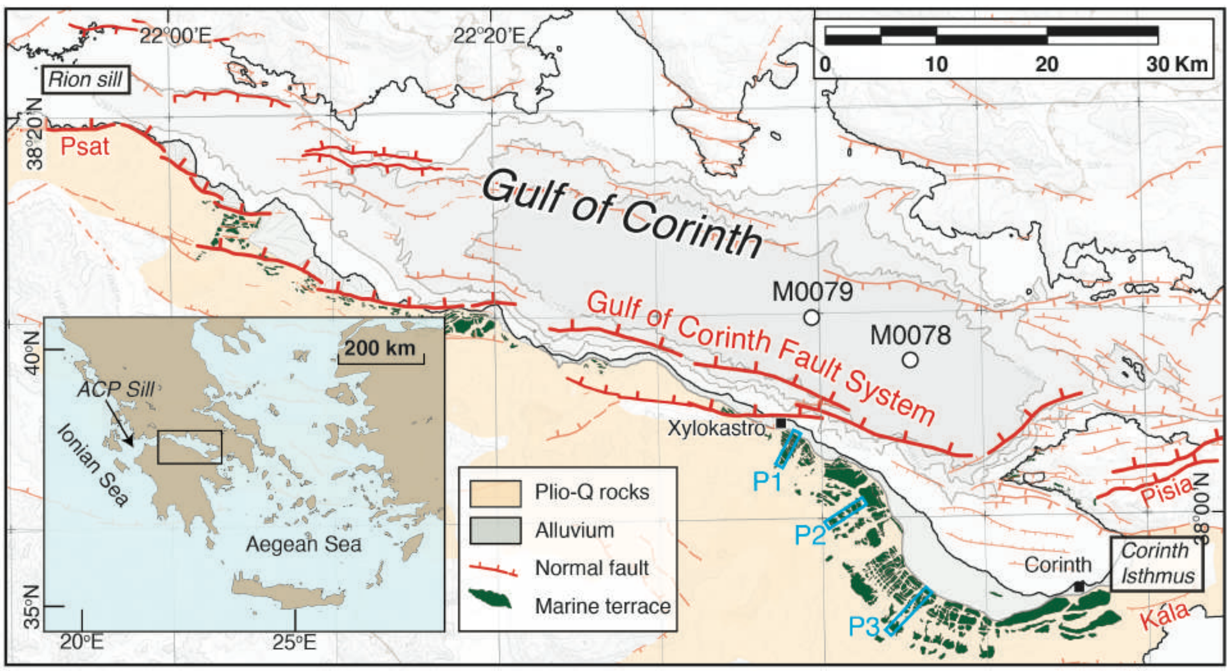

Figure 4. Tectonomorphology of the Gulf of Corinth. Map showing the main features of the Gulf of Corinth, including the active faults, marine terraces, profile locations used in the inversion and connections to the Ionian Sea (Rion Sill) and Aegean Sea (Corinth Isthmus). M0078 and M0079 indicate the IODP-381 sedimentary coring locations (McNeill et al., 2019). Psat = Psathopyrgos Fault, Pisia = Pisia Fault, Kala = Kalamaki Fault. Modified from de Gelder et al. (2019).

The individual profile inversions mostly constrain paleo sea/lake level for profile 1 (Fig. 5a), because it has the highest uplift rate and contains most terraces. The other two profiles provide limited constraints on paleo sea/lake level when inverted individually (Fig. 5b/c), but together with profile 1 they provide a much narrower range (Fig. 5d). The cumulative RMS misfit for the individual inversions (28 m) is slightly better than for the joint inversion (46 m), but there are no major visible differences between the terrace sequence profiles for the two inversions, and apart from the highest terrace of profile 2 (Fig. 5b) the terrace sequences are all near perfectly reconstructed. The three profiles show variations in initial slopes that are in line with the overall morphology, but have similar wave base depths and erosion rates (Fig. 5e). The inverted parameter ranges mostly remain the same between the individual and joint inversion, with exception of the uplift rates for profiles 2 and 3 that became a little lower for the joint inversion. As for the sea-/lake-level inversion, all the other parameter ranges become narrower for the joint inversion (Fig. 5e).

The inverted sea-/lake-level history (Fig. 5d) shows a few particular features. To a first order fluctuations resemble global sea-level trends, with relatively fast periods of sea-/lake-level rise prior to major sea-level highstands, followed by long periods of slow sea-/lake-level fall (Fig. 1c). Yet, unlike global sea-level trends, there are several periods of prolonged stability, in particular around 180-200 ka and 275-300 ka, and possibly also around 75-95 ka and 360-370 ka. In addition, glacial periods are often surprisingly poorly resolved, like during the period 20-75 ka or 160-180 ka In the last section we discuss our interpretation of these trends, and show how they provide insightful arguments to decipher the relation between water level, fault activity, paleoclimate and tectonics.

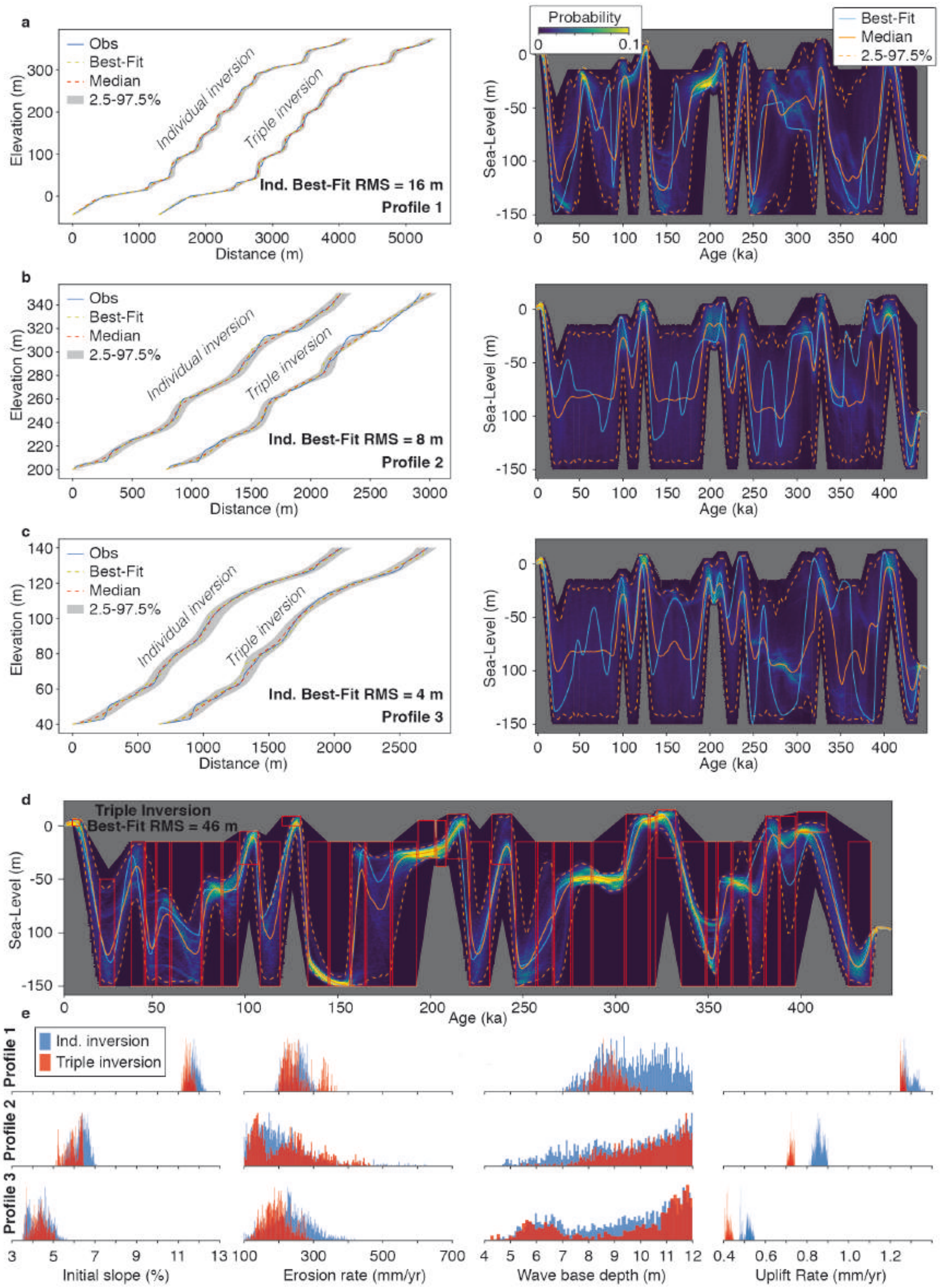

Figure 5. Inversion of SE Corinth Rift marine terrace sequence. a-c) Observed topography (left) from 3 different profiles in the SE Corinth Rift (locations see Fig. S3), together with the modeled best-fit, median, 2.5% and 97.5% percentile profiles for both an individual profile inversion and a joint inversion of the three profiles (horizontally offset by an arbitrary value). Corresponding probabilistic sea/lake-level ranges for the individually inverted profiles are given

on the right, **d)** Probabilistic sea/lake-level history from joint inversion, **e)** Resulting parameter ranges from both individual and joint profile inversions

6 Discussion

6.1 Inversion of marine terrace sequences

In the examples above, we showed how to assess paleo sea-level variations, and simultaneously extract quantified metrics for morphotectonics and hydrodynamics, from the geometry of marine terrace sequences. Using a probabilistic inversion methodology set in a Bayesian framework, we avoid the simplifications of bijective approaches in which a single marine terrace is always linked to a single sea-level highstand and vice-versa (e.g. Pastier et al., 2019; Malatesta et al., 2021). By considering a full sea-level curve and its possible variability, it is possible to provide quantitative constraints on highstands, lowstands, sea-level rise and fall, filling the observational gap for time periods for which field measurements are scarce. We admit that some model simplifications and approximations may alter our interpretations. In particular, we neglect subaerial erosion, and kept uplift rate, erosion rate, initial slope and wave base depth parameters time-constant for each individual sampled paleo sea level curve. Both could be fine-tuned in future developments.

Many paleo sea-level studies that use geomorphic/geologic observations tend to have a confirmation bias regarding sea-level curves, and propose refinements of paleo sea-level estimates to sub-m scale (e.g. Murray-Wallace, 2002; Roberts et al., 2012) or uplift rates to precisions of ~0.01 mm/yr (e.g. Pedoja et al., 2018; Meschis et al., 2022). In this study, we take a step back by allowing more freedom to possible paleo sea-level variations, as well as uplift rate, erosion rate, initial slope and wave base depth, to provide a more reliable way to translate morphologic observations to paleo sea-level constraints. For instance, the low uplift rate examples from the Corinth Rift (Fig. 5b, c) and Santa Cruz (Fig. S2) reveal very little about paleo sea/lake levels, even if the uplift rate is roughly known. As a marine terrace is formed over several sea-level cycles, the resulting terrace width and height will depend on all those cycles, as well as wave base depths, erosion rates and initial slopes, all of which are generally poorly constrained. Even in the hypothetical case that these parameters are known (Fig. 2), there is still a wide spectrum of sea-level histories that could have created the specific morphology of a marine terrace sequence. It suggests that estimating paleo sea-level based on the comparison of a present-day landform to a paleo-landform (Rovere et al., 2016), may be too simplistic in many cases, at least for erosive marine terraces. Although uncertainties that we provide on paleo sea-level are much larger than what calculations based on hydrodynamic ranges would suggest (Lorchsteid and Rovere, 2019), we do consider them to be reliable as they take in a large number of unknowns.

Although here we focused on erosive marine terraces to develop a proof of concept, a promising avenue is to apply this inversion method to bio-constructed (coral reef) terraces, which tend to be better dated (e.g. Pedoja et al., 2014; Hibbert et al., 2016) and for which modelling routines also exist (e.g. Toomey et al., 2013; Pastier et al., 2019). One of our key findings is that inverting multiple profiles simultaneously provides much better paleo sea-level constraints than focusing on individual profiles (Figs. 2, 5). The global archive of paleo-shorelines (Fig. 1a) presents a huge potential for such multi-profile marine terrace inversions. This massive inversion would not only lead to improved estimates of local relative sea-level histories, but may also complement studies on glacio-isostatic adjustments that are relevant to a global sea-level perspective.

6.2 Tectono-hydro-climatic processes in the Gulf of Corinth

The results for the joint inversion of the 3 profiles in the Gulf of Corinth allow for a more detailed look into sea- and lake-level fluctuations within a (semi-)isolated basin. Figure 6 compares our inverted sea-lake level to the stratigraphy, facies and pollen content within two sedimentary cores from the sea floor of the central basin (McNeil et al., 2019; Gawthorpe et al., 2022; Kafetzidou et al., 2023). Based on those combined datasets, we propose that the main hydroclimatic modes that have occurred in the Gulf of Corinth throughout the past 450 ka, are 1) marine Gulf of Corinth, 2) transitional Gulf of Corinth or overfilled Lake Corinth and 3) underfilled Lake Corinth. The first 2 of those have been proposed before based on sedimentary cores (McNeill et al., 2019; Gawthorpe et al., 2022), whereas we base the occurrence of intervals with an underfilled Lake Corinth on our marine/lake terrace inversion.

The major peaks in our reconstructed sea/lake-level curve occurred during interglacial sea-level highstands, when sea level in the Gulf of Corinth was similar to eustatic sea level (marine mode M). Sedimentary cores indicate marine conditions (McNeill et al., 2019), the corresponding stratal packages are bioturbated, and associated sedimentary facies are types FA1 and FA6 (Fig. 6; see caption for facies description). From pollen records, the typical reconstructed biomes are cool mixed evergreen needleleaf and deciduous broadleaf forests, indicating relatively warm and wet conditions with low amounts of steppic taxa (Kafetzidou et al., 2023; Fig. 6).

We interpret the interstadial periods around 75-95 ka, 180-200 ka, 275-300 ka and 360-370 ka as periods with an overfilled Lake Corinth, possibly with some marine incursions indicating a transitional Gulf of Corinth (T/O mode). This would explain the prolonged sea-/lake-level stability, during interstadial periods when eustatic sea-level fluctuated by tens of meters (e.g. Spratt and Lisiecki, 2016; De Gelder et al., 2022). In that case, sea-/lake-level elevations would correspond to the paleo-sill depth of the Rion Sill and/or Corinth Isthmus (white line, Fig. 6). Within the sedimentary cores, these periods are mostly characterized by laminated stratal packages, and associated sedimentary facies are types FA2, FA3 and FA4 (Fig. 6; see caption for facies description). The occurrence of marine incursions into Lake Corinth during these interstadial periods is suggested by dated corals of ~76 ka, ~178 ka and ~201 ka (Roberts et al., 2009; Houghton et al., 2003) as well as the white, aragonite-rich laminations of FA3 and FA4. In other locations such laminations have been linked to (seasonal) mixing of marine and non-marine surface waters (Sondi & Juracic, 2010; Roeser et al., 2016).

The glacial periods are characterized by relatively low sea/lake-level elevations, possibly even down to the lower limit of -150 m we used in the inversion. We interpret these periods as underfilled Lake Corinth conditions (U mode), during which water inflow was lower than water evaporation within the lake, and lake level fell down to tens of meters below the sill depth. Sedimentary cores indicate non-marine conditions (McNeill et al., 2019), the corresponding stratal packages are mostly bedded and associated sedimentary facies are types FA5 and FA11 (Fig. 6; see caption for facies description). Reconstructed biomes from pollen suggest an increase in open vegetation such as grassland and steppe communities under colder and drier conditions (Kafetzidou et al., 2023; Fig. 6), matching reconstructed periods of lake underfilling. In general the inverted resolution of the lake-level elevation is much lower for these periods, with large probabilistic ranges. We attribute this to the occurrence of rapid lake-level fluctuations, like in other isolated E-Mediterranean water bodies such as the Dead Sea (Stein et al., 2010) and Lake Van (Turkey; Landmann et al., 1996). In such environments, the lake level is determined by the budget between runoff and evaporation, and quick variations are expected. Alternatively, this could also be due to the fact that terraces formed during low sea/lake level get increasingly eroded during transgressions.

The interstadial periods with prolonged sea-/lake-level stability also allow for a possible reconstruction of sill depths through time (white lines, Fig. 6). The westernmost sill, the Acheloos-Cape Pappas Sill (Fig. 4), is currently at a depth of ~45-48 m. While there are no major faults there, we can't exclude slow subsidence or uplift at a few tenths of mm/yr, cumulating to a few tens of meters on the 100 kyr time scale. The Rion Sill, at the western entrance to the Gulf of Corinth, is currently at ~62 m depth (Perissoratis et al., 2000). As it is located in the hanging wall of the Psathopyrgos Fault (Fig. 5), active since at least the past ~200 ka (Houghton et al., 2003), the Rion Sill was unlikely deeper in the past. We reconstruct the Rion Sill depth assuming marine incursions around ~76 ka (Roberts et al., 2009) took place through this sill, and the Rion Sill was not lower than sea/lake level during the overfilled/transitional interval around ~200 ka. Extrapolating the trend, it would make sense for the older connections between Lake/Gulf of Corinth and the open sea to have occurred primarily through the Corinth Isthmus at the eastern end of the Gulf of Corinth.

The Corinth Isthmus is currently at an elevation of ~80 m, and has been uplifted through the Pisia Fault, Kalamaki Fault and/or a regional uplift (Armijo et al., 1996; Roberts et al., 2009; Caterina et al., 2022). We reconstruct the Corinth Isthmus depth assuming lake/sea level during overfilled/transitional intervals around ~290 and ~360 ka correspond to the Corinth Isthmus depth, and the isthmus was not lower than sea/lake level during the overfilled/transitional interval around ~200 ka. Extrapolating this trend fits with the current Corinth Isthmus elevation of ~80 m. The isthmus elevation before ~360 ka is difficult to constrain from our data, but was possibly shallower before, given the small amount of marine sediments deposited around the ~400 ka interglacial period, and the lack of deposits within the Isthmus stratigraphy older than ~350 ka (Collier and Dart, 1991; Caterina et al., 2022). Our reconstruction of both Rion Sill and Corinth Isthmus fits with the sedimentary interpretation of a tidal strait around ~300 ka at the isthmus, with marine connections on both ends of the Gulf of Corinth (Caterina et al., 2022).

Our exploration of sea-/lake-level variations in the Gulf of Corinth demonstrates the strength of using marine terrace sequence inversion. Although several questions remain – like the effects of erosion and sedimentation on sill evolution, or the effects of non-constant uplift rates of the marine terrace sequences – we are able to provide a solid framework that can explain several different tectonic and hydro-climatic processes simultaneously. We distinguish 4 different hydroclimatic modes of for the Lake/Gulf of Corinth, that have probably also occurred in other (semi-)isolated basins like the Sea of Marmara or the Carioco Basin. Marine and transitional modes will most likely depend on eustatic sea-level elevations and sill depths, whereas over- or underfilled lakes likely depend on sill depths and local climatic conditions. For the Corinth Lake we show that this transition from over- to underfilled lakes occurs during changes from interstadial to glacial periods, and is accompanied by changes in vegetation that imply drier conditions.

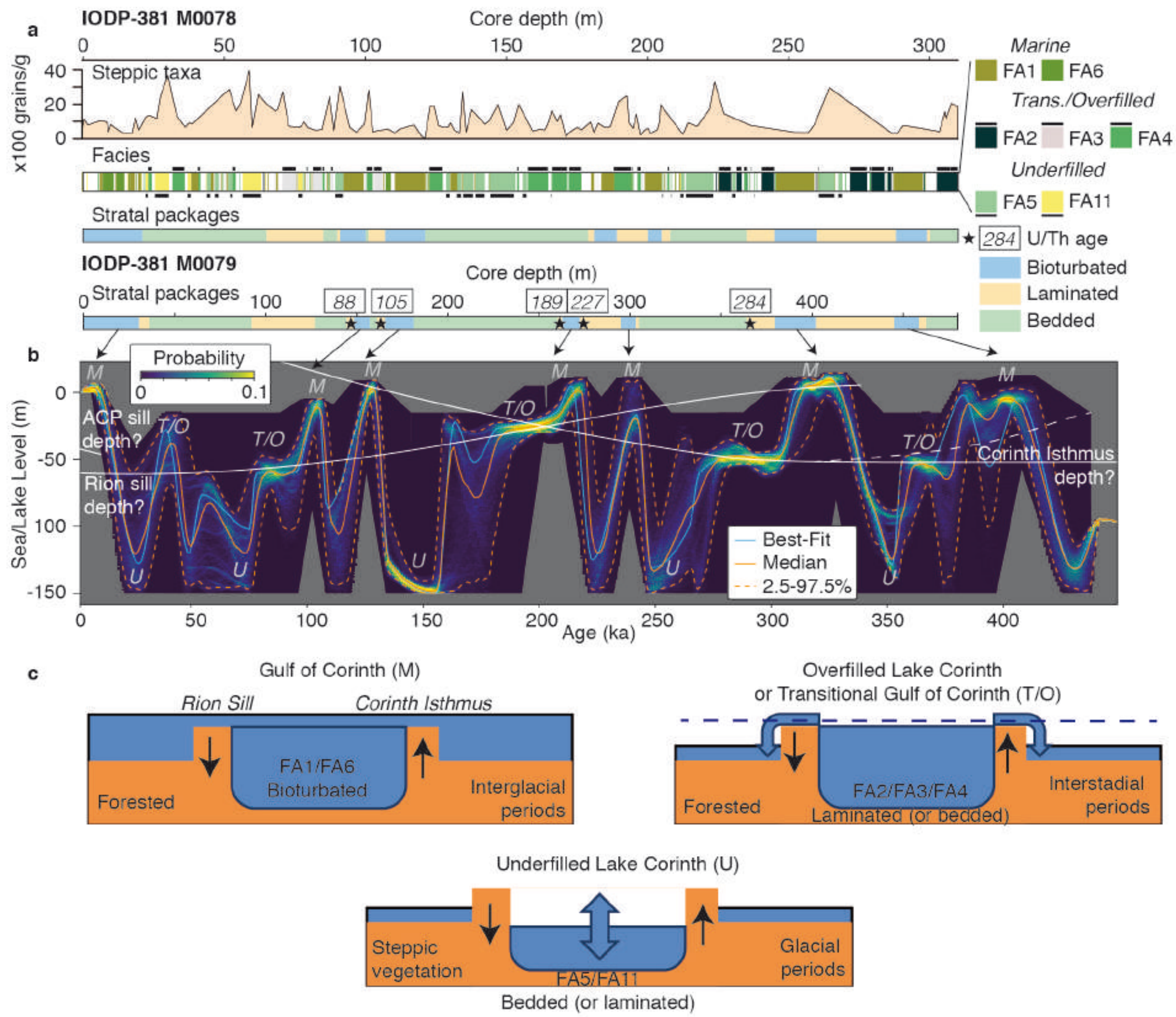

Figure 6. Comparison of sea-/lake-level reconstruction to other datasets. a) Comparison to IODP-381 cores M0078 and M0079, with steppic taxa from Kafetzidou et al. (2023), facies from McNeill et al. (2019) and stratal packages with U/Th ages from Gawthorpe et al. (2022). FA1: homogenous mud, FA2: greenish gray mud with dark gray to black silty-to-sandy beds (cm-scale), FA3: light gray to white sub-mm laminations (cc or aragonite) alternating with mud–silt beds, FA4: laminated greenish gray to gray mud with muddy beds, FA5: greenish gray mud with homogeneous cm thick gray mud beds, FA6: green bedded partly bioturbated mud, silt and sand, FA11: interbedded mud/silt and cm thick sand beds. **b)** Inversion result from Fig. 5d with proposed sill/isthmus elevations, marking periods with marine (M), transitional or overfilled (T/O) and underfilled (U) hydroclimatic modes. **c)** Schematic illustrations of the different hydroclimatic modes in the Lake/Gulf of Corinth.

7 Conclusions

In this study we demonstrated the use of a probabilistic inversion approach to decipher the formation of marine terrace sequences in general, and the tectonic and hydro-climatic evolution of (semi-)isolated basins in particular. With this approach, we provide the tools (see below) to simultaneously estimate past sea-level variations, uplift rates, erosion rates, initial slopes and wave heights.

From synthetic tests, benchmarking on a terrace sequence near Santa Cruz marine terrace sequence, and application to the sequence in the SE Gulf of Corinth, our results bring a theoretical advance by showing that : 1) Paleo sea-level and other parameter ranges can be better constrained from sequences that are uplifting at higher rates compared to lower rates, and better constrained from a joint inversion of multiple profiles than from inversion of a single profile. 2) Uplift rates, sea-level variations and wave erosion parameters are intricately linked. By allowing more freedom to possible ranges of all the relevant parameters, we provide a more reliable way to translate morphologic observations to paleo sea-level constraints. Resulting uncertainties may be higher compared to 'classic' approaches of comparing present to past shoreline elevations, but are more realistic. 3) Probabilistic inversion of marine terrace sequences is a powerful method, applicable to a large portion of the world's coastlines to disentangle tectonic and hydro-climatic processes.

By applying our method to a complex case -the semi-isolated Gulf of Corinth (Greece)- we found that eustatic sea-level and tectonically changing sill depths drive marine and transitional phases during interglacial and interstadial periods, respectively. Wetter and drier conditions drive over- and underfilling of Lake Corinth during interstadial and glacial periods, respectively. We expect such transitions to be different for each unique tectono-hydro-climatic setting, with our inversion approach providing a new way to decipher such geomorphic Rosetta stones.

Acknowledgments

This study has been funded by the European Union horizon 2020 research and innovation program under grant agreement 716542. Furthermore, GdG acknowledges postdoctoral funding from the IRD and the Manajemen Talenta BRIN fellowship program. GdG likes to thank Katerina Kouli for sharing her pollen data, and other IODP-381 expedition members, as well as David Fernández-Blanco, Robin Lacassin and Rolando Armijo, for the many fruitful discussions on the Corinth Rift.

Open Research

The marine terrace inversion code used in this study can be found at https://github.com/ginodegelder/Rosetta.

References

Aksu, A. E., Hiscott, R. N., & Dogan, Y. (1999). Oscillating Quaternary water levels of the Marmara Sea and vigorous outflow into the Aegean Sea from the Marmara Sea–Black Sea drainage corridor. *Marine Geology*, *153*(1-4), 275-302.

Andersen, M. B., Stirling, C. H., Potter, E. K., Halliday, A. N., Blake, S. G., McCulloch, M. T., ... & O'Leary, M. J. (2010). The timing of sea-level high-stands during Marine Isotope Stages 7.5 and 9: Constraints from the uranium-series dating of fossil corals from Henderson Island. *Geochimica et Cosmochimica Acta*, *74*(12), 3598-3620.

Anderson, R.S., Densmore, A.L., Ellis, M.A., 1999. The generation and degradation of marine terraces. Basin Res. 11 (1), 7e19.

Anderson, R. S., & Menking, K. M. (1994). The Quaternary marine terraces of Santa Cruz, California: Evidence for coseismic uplift on two faults. *Geological Society of America Bulletin*, *106*(5), 649-664.

Armijo, R., Meyer, B. G. C. P., King, G. C. P., Rigo, A., & Papanastassiou, D. (1996). Quaternary evolution of the Corinth Rift and its implications for the Late Cenozoic evolution of the Aegean. *Geophysical Journal International*, *126*(1), 11-53.

Austermann, J., Mitrovica, J. X., Huybers, P., & Rovere, A. (2017). Detection of a dynamic topography signal in last interglacial sea-level records. *Science Advances*, *3*(7), e1700457.

Batchelor, C. L., Margold, M., Krapp, M., Murton, D. K., Dalton, A. S., Gibbard, P. L., ... & Manica, A. (2019). The configuration of Northern Hemisphere ice sheets through the Quaternary. *Nature communications*, *10*(1), 3713.

Beckers, A., Beck, C., Hubert-Ferrari, A., Tripsanas, E., Crouzet, C., Sakellariou, D., ... & De Batist, M. (2016). Influence of bottom currents on the sedimentary processes at the western tip of the Gulf of Corinth, Greece. *Marine Geology*, *378*, 312-332.

Bloom, A. L., & Yonekura, N. (1990). Graphic analysis of dislocated Quaternary shorelines. *Sea-level change*, 104-115.

Bradley, W. C. (1957). Origin of marine-terrace deposits in the Santa Cruz area, California. *Geological Society of America Bulletin*, *68*(4), 421-444.

Bradley, W. C., & Addicott, W. O. (1968). Age of first marine terrace near Santa Cruz, California. *Geological Society of America Bulletin*, *79*(9), 1203-1210.

Brown, E. T., & Bourles, D. L. (2002). Use of a new 10Be and 26Al inventory method to date marine terraces, Santa Cruz, California, USA: Comment and Reply: COMMENT. *Geology*, *30*(12), 1147-1148.

Caterina, B., Rubi, R., & Hubert-Ferrari, A. (2023). Stratigraphic architecture, sedimentology and structure of the Middle Pleistocene Corinth Canal (Greece). *Geological Society, London, Special Publications*, *523*(1), 279-304.

Chappell, J., & Shackleton, N. (1986). Oxygen isotopes and sea level. *Nature*, *324*(6093), 137-140.

Chauveau, D., Pastier, A.-M., de Gelder, G., Husson, L., Authemayou, C., Pedoja, K. et al. (2024) Unravelling the morphogenesis of coastal terraces at Cape Laundi (Sumba Island, Indonesia): Insights from numerical models. *Earth Surface Processes and Landforms*, 49(2), 549–566.

Collier, R. L., & Dart, C. J. (1991). Neogene to Quaternary rifting, sedimentation and uplift in the Corinth Basin, Greece. *Journal of the Geological Society*, *148*(6), 1049-1065.

Creveling, J. R., Mitrovica, J. X., Clark, P. U., Waelbroeck, C., & Pico, T. (2017). Predicted bounds on peak global mean sea level during marine isotope stages 5a and 5c. *Quaternary Science Reviews*, *163*, 193-208.

Dalton, A. S., Finkelstein, S. A., Forman, S. L., Barnett, P. J., Pico, T., & Mitrovica, J. X. (2019). Was the Laurentide Ice Sheet significantly reduced during marine isotope stage 3?. *Geology*, *47*(2), 111-114.

Dalton, A. S., Pico, T., Gowan, E. J., Clague, J. J., Forman, S. L., McMartin, I., ... & Helmens, K. F. (2022). The marine δ18O record overestimates continental ice volume during Marine Isotope Stage 3. *Global and Planetary Change*, *212*, 103814.

De Gelder, G., Fernández-Blanco, D., Melnick, D., Duclaux, G., Bell, R. E., Jara-Muñoz, J., ... & Lacassin, R. (2019). Lithospheric flexure and rheology determined by climate cycle markers in the Corinth Rift. *Scientific Reports*, *9*(1), 4260.

De Gelder, G., Jara-Munoz, J., Melnick, D., Fernández-Blanco, D., Rouby, H., Pedoja, K., ... & Lacassin, R. (2020). How do sea-level curves influence modeled marine terrace sequences?. *Quaternary Science Reviews*, *229*, 106132.

De Gelder, G., Husson, L., Pastier, A. M., Fernández-Blanco, D., Pico, T., Chauveau, D., ... & Pedoja, K. (2022). High interstadial sea levels over the past 420ka from the Huon Peninsula, Papua New Guinea. *Communications Earth & Environment*, *3*(1), 256.

De Gelder, G., Solihuddin, T., Utami, D. A., Hendrizan, M., Rachmayani, R., Chauveau, D., ... & Cahyarini, S. Y. (2023). Geodynamic control on Pleistocene coral reef development: insights from northwest Sumba Island (Indonesia). *Earth Surface Processes and Landforms*, *48*(13), 2536-2553.

Derricourt, R. (2005). Getting "Out of Africa": sea crossings, land crossings and culture in the hominin migrations. *Journal of world prehistory*, *19*, 119-132.

Dutton, A., Carlson, A. E., Long, A. J., Milne, G. A., Clark, P. U., DeConto, R., ... & Raymo, M. E. (2015). Sea-level rise due to polar ice-sheet mass loss during past warm periods. *science*, *349*(6244), aaa4019.

Dyer, B., Austermann, J., D'Andrea, W. J., Creel, R. C., Sandstrom, M. R., Cashman, M., ... & Raymo, M. E. (2021). Sea-level trends across The Bahamas constrain peak last interglacial ice melt. *Proceedings of the National Academy of Sciences*, *118*(33), e2026839118.

Fernández-Blanco, D., de Gelder, G., Lacassin, R., & Armijo, R. (2019). A new crustal fault formed the modern Corinth Rift. *Earth-Science Reviews*, *199*, 102919.

Gallagher, K., Charvin, K., Nielsen, S., Sambridge, M., & Stephenson, J. (2009). Markov chain Monte Carlo (MCMC) sampling methods to determine optimal models, model resolution and model choice for Earth Science problems. *Marine and Petroleum Geology*, *26*(4), 525-535.

Gawthorpe, R. L., Fabregas, N., Pechlivanidou, S., Ford, M., Collier, R. E. L., Carter, G. D., ... & Shillington, D. J. (2022). Late Quaternary mud‐dominated, basin‐floor sedimentation of the Gulf of Corinth, Greece: Implications for deep‐water depositional processes and controls on syn‐rift sedimentation. *Basin Research*, *34*(5), 1567-1600.

Gowan, E. J., Zhang, X., Khosravi, S., Rovere, A., Stocchi, P., Hughes, A. L., ... & Lohmann, G. (2021). A new global ice sheet reconstruction for the past 80 000 years. *Nature communications*, *12*(1), 1199.

Guilcher, A., 1974. Les «rasas»: un problème de morphologie littorale générale. *Annales de Géographie*, 83, 1–33.

Hay, C., Mitrovica, J. X., Gomez, N., Creveling, J. R., Austermann, J., & Kopp, R. E. (2014). The sea-level fingerprints of ice-sheet collapse during interglacial periods. *Quaternary Science Reviews*, *87*, 60-69.

Hibbert, F. D., Rohling, E. J., Dutton, A., Williams, F. H., Chutcharavan, P. M., Zhao, C., & Tamisiea, M. E. (2016). Coral indicators of past sea-level change: A global repository of U-series dated benchmarks. *Quaternary Science Reviews*, *145*, 1-56.

Houghton, S. L., Roberts, G. P., Papanikolaou, I. D., McArthur, J. M., & Gilmour, M. A. (2003). New 234U-230Th coral dates from the western Gulf of Corinth: Implications for extensional tectonics. *Geophysical Research Letters*, *30*(19).

Husson, L., Pastier, A.-M., Pedoja, K., Elliot, M., Paillard, D., Authemayou, C., et al., 2018. Reef carbonate productivity during quaternary sea level oscillations. Geochem. Geophys. Geosyst. 19 (4), 1148e1164.

Jara-Muñoz, J., Melnick, D., Pedoja, K., & Strecker, M. R. (2019). TerraceM-2: A Matlab® interface for mapping and modeling marine and lacustrine terraces. *Frontiers in Earth Science*, 255.

Johnson, M. E., & Libbey, L. K. (1997). Global review of upper Pleistocene (substage 5e) rocky shores: tectonic segregation, substrate variation, and biological diversity. *Journal of Coastal Research*, 297-307.

Kafetzidou, A., Fatourou, E., Panagiotopoulos, K., Marret, F., & Kouli, K. (2023). Vegetation Composition in a Typical Mediterranean Setting (Gulf of Corinth, Greece) during Successive Quaternary Climatic Cycles. *Quaternary*, *6*(2), 30.

Kennedy, G. L., Lajoie, K. R., & Wehmiller, J. F. (1982). Aminostratigraphy and faunal correlations of late Quaternary marine terraces, Pacific Coast, USA. *Nature*, *299*(5883), 545-547.

Kopp, R. E., Simons, F. J., Mitrovica, J. X., Maloof, A. C., & Oppenheimer, M. (2009). Probabilistic assessment of sea level during the last interglacial stage. *Nature*, *462*(7275), 863-867.

Landmann, G., Reimer, A., & Kempe, S. (1996). Climatically induced lake level changes at Lake Van, Turkey, during the Pleistocene/Holocene transition. *Global Biogeochemical Cycles*, *10*(4), 797-808.

Lajoie, K. R., Wehmiller, J. F., Kvenvolden, K. A., Peterson, E., & White, R. H. (1975). Correlation of California marine terraces by amino acid stereochemistry. In *Geological Society of America Abstracts with Programs* (Vol. 7, No. 3, pp. 338-339).

Lajoie, K.R., 1986. Coastal tectonics. In: Press, N.A. (Ed.), Active Tectonics. National Academic Press, Washington DC, pp. 95e124.

Lambeck, K., & Chappell, J. (2001). Sea level change through the last glacial cycle. *Science*, *292*(5517), 679-686.

Leclerc, F., & Feuillet, N. (2019). Quaternary coral reef complexes as powerful markers of long-term subsidence related to deep processes at subduction zones: Insights from Les Saintes (Guadeloupe, French West Indies). *Geosphere*, *15*(4), 983-1007.

Lorscheid, T., & Rovere, A. (2019). The indicative meaning calculator–quantification of paleo sea-level relationships by using global wave and tide datasets. *Open Geospatial Data, Software and Standards*, *4*, 1-8.

Malatesta, L. C., Finnegan, N. J., Huppert, K. L., & Carreño, E. I. (2022). The influence of rock uplift rate on the formation and preservation of individual marine terraces during multiple sea-level stands. *Geology*, *50*(1), 101-105.

Marra, F., Sevink, J., Tolomei, C., Vannoli, P., Florindo, F., Jicha, B. R., & La Rosa, M. (2023). New age constraints on the MIS 9–MIS 5.3 marine terraces of the Pontine Plain (central Italy) and implications for global sea levels. *Quaternary Science Reviews*, *300*, 107866.

Matsumoto, H., Young, A. P., & Carilli, J. E. (2022). Modeling the relative influence of environmental controls on marine terrace widths. *Geomorphology*, *396*, 107986.

McNeill, L. C., Shillington, D. J., Carter, G. D., Everest, J. D., Gawthorpe, R. L., Miller, C., ... & Green, S. (2019). High-resolution record reveals climate-driven environmental and sedimentary changes in an active rift. *Scientific Reports*, *9*(1), 3116.

Medina-Elizalde, M. (2013). A global compilation of coral sea-level benchmarks: implications and new challenges. *Earth and Planetary Science Letters*, *362*, 310-318.

Meschis, M., Roberts, G. P., Robertson, J., Mildon, Z. K., Sahy, D., Goswami, R., ... & Iezzi, F. (2022). Out of phase Quaternary uplift-rate changes reveal normal fault interaction, implied by deformed marine palaeoshorelines. *Geomorphology*, *416*, 108432.

Mosegaard, K., & Sambridge, M. (2002). Monte Carlo analysis of inverse problems. *Inverse problems*, *18*(3), R29.

Murray-Wallace, C. V. (2002). Pleistocene coastal stratigraphy, sea-level highstands and neotectonism of the southern Australian passive continental margin—a review. *Journal of Quaternary Science: Published for the Quaternary Research Association*, *17*(5-6), 469-489.

Ott, R. F., Gallen, S. F., Wegmann, K. W., Biswas, R. H., Herman, F., & Willett, S. D. (2019). Pleistocene terrace formation, Quaternary rock uplift rates and geodynamics of the Hellenic Subduction Zone revealed from dating of paleoshorelines on Crete, Greece. *Earth and Planetary Science Letters*, *525*, 115757.

Pastier, A.-M., Husson, L., Pedoja, K., Bezos, A., Authemayou, C., Arias-Ruiz, C., Cahyarini, S.Y. (2019). Genesis and architecture of sequences of quaternary coral reef terraces: Insights from numerical models. *Geochem. Geophy. Geosyst.*, 20 (8), 4248e4272.

Pedoja, K., Husson, L., Regard, V., Cobbold, P. R., Ostanciaux, E., Johnson, M. E., ... & Delcaillau, B. (2011). Relative sea-level fall since the last interglacial stage: are coasts uplifting worldwide?. *Earth-Science Reviews*, *108*(1-2), 1-15.

Pedoja, K., Husson, L., Johnson, M. E., Melnick, D., Witt, C., Pochat, S., ... & Garestier, F. (2014). Coastal staircase sequences reflecting sea-level oscillations and tectonic uplift during the Quaternary and Neogene. *Earth-Science Reviews*, *132*, 13-38.

Pedoja, K., Jara-Muñoz, J., De Gelder, G., Robertson, J., Meschis, M., Fernández-Blanco, D., ... & Pinel, B. (2018). Neogene-Quaternary slow coastal uplift of Western Europe through the perspective of sequences of strandlines from the Cotentin Peninsula (Normandy, France). *Geomorphology*, *303*, 338-356.

Perg, L. A., Anderson, R. S., & Finkel, R. C. (2001). Use of a new 10Be and 26Al inventory method to date marine terraces, Santa Cruz, California, USA. *Geology*, *29*(10), 879-882.

Perissoratis, C., Piper, D. J. W., & Lykousis, V. (2000). Alternating marine and lacustrine sedimentation during late Quaternary in the Gulf of Corinth rift basin, central Greece. *Marine Geology*, *167*(3-4), 391-411.

Pico, T., Mitrovica, J. X., Ferrier, K. L., & Braun, J. (2016). Global ice volume during MIS 3 inferred from a sea-level analysis of sedimentary core records in the Yellow River Delta. *Quaternary Science Reviews*, *152*, 72-79.

Pirazzoli, P.A., 2005. Marine terraces. In: Schwartz, M.L. (Ed.), Encyclopedia of Coastal Science. Springer Netherlands, Dordrecht, pp. 632-633.

Railsback, L. B., Gibbard, P. L., Head, M. J., Voarintsoa, N. R. G., & Toucanne, S. (2015). An optimized scheme of lettered marine isotope substages for the last 1.0 million years, and the climatostratigraphic nature of isotope stages and substages. *Quaternary Science Reviews*, *111*, 94-106.

Regard, V., Pedoja, K., De La Torre, I., Saillard, M., Corte_s-Aranda, J., Nexer, M., 2017. Geometrical trends within sequences of Pleistocene marine terraces: selected examples from California, Peru, Chile and New-Zealand. *Zeitschrift Fur Geomorphologie* 61 (1), 53e73.

Roberts, G. P., Houghton, S. L., Underwood, C., Papanikolaou, I., Cowie, P. A., van Calsteren, P., ... & McArthur, J. M. (2009). Localization of Quaternary slip rates in an active rift in 105 years: An example from central Greece constrained by 234U-230Th coral dates from uplifted paleoshorelines. *Journal of Geophysical Research: Solid Earth*, *114*(B10).

Roberts, D. L., Karkanas, P., Jacobs, Z., Marean, C. W., & Roberts, R. G. (2012). Melting ice sheets 400,000 yr ago raised sea level by 13 m: Past analogue for future trends. *Earth and Planetary Science Letters*, *357*, 226-237.

Roeser, P., Franz, S. O., & Litt, T. (2016). Aragonite and calcite preservation in sediments from Lake Iznik related to bottom lake oxygenation and water column depth. *Sedimentology*, *63*(7), 2253-2277.

Rosenbloom, N. A., & Anderson, R. S. (1994). Hillslope and channel evolution in a marine terraced landscape, Santa Cruz, California. *Journal of Geophysical Research: Solid Earth*, *99*(B7), 14013-14029.

Rovere, A., Raymo, M. E., Vacchi, M., Lorscheid, T., Stocchi, P., Gomez-Pujol, L., ... & Hearty, P. J. (2016). The analysis of Last Interglacial (MIS 5e) relative sea-level indicators: Reconstructing sea-level in a warmer world. *Earth-Science Reviews*, *159*, 404-427.

Rovere, A., Ryan, D. D., Vacchi, M., Dutton, A., Simms, A. R., & Murray-Wallace, C. V. (2023). The World Atlas of Last Interglacial Shorelines (version 1.0). *Earth System Science Data*, *15*(1), 1-23.

Schellmann, G., & Radtke, U. (2004). A revised morpho-and chronostratigraphy of the Late and Middle Pleistocene coral reef terraces on Southern Barbados (West Indies). *Earth-Science Reviews*, *64*(3-4), 157-187.

Shakun, J. D., Lea, D. W., Lisiecki, L. E., & Raymo, M. E. (2015). An 800-kyr record of global surface ocean δ18O and implications for ice volume-temperature coupling. *Earth and Planetary Science Letters*, *426*, 58-68.

Siddall, M., Smeed, D. A., Hemleben, C., Rohling, E. J., Schmelzer, I., & Peltier, W. R. (2004). Understanding the Red Sea response to sea level. *Earth and Planetary Science Letters*, *225*(3-4), 421-434.

Sondi, I., & Juračić, M. (2010). Whiting events and the formation of aragonite in Mediterranean Karstic Marine Lakes: new evidence on its biologically induced inorganic origin. *Sedimentology*, *57*(1), 85-95.

Spratt, R. M., & Lisiecki, L. E. (2016). A Late Pleistocene sea level stack. *Climate of the Past*, *12*(4), 1079-1092.

Stein, M., Torfstein, A., Gavrieli, I., & Yechieli, Y. (2010). Abrupt aridities and salt deposition in the post-glacial Dead Sea and their North Atlantic connection. *Quaternary Science Reviews*, *29*(3-4), 567-575.

Stirling, C. H., Esat, T. M., Lambeck, K., McCulloch, M. T., Blake, S. G., Lee, D. C., & Halliday, A. N. (2001). Orbital forcing of the marine isotope stage 9 interglacial. *Science*, *291*(5502), 290-293.

Strobl, M., Hetzel, R., Fassoulas, C., & Kubik, P. W. (2014). A long-term rock uplift rate for eastern Crete and geodynamic implications for the Hellenic subduction zone. *Journal of Geodynamics*, *78*, 21-31.

Sunamura, T. (1992). *Geomorphology of Rocky Coasts*, vol. 3. John Wiley & Son Ltd.

Tawil-Morsink, K., Austermann, J., Dyer, B., Dumitru, O. A., Precht, W. F., Cashman, M., ... & Raymo, M. E. (2022). Probabilistic investigation of global mean sea level during MIS 5a based on observations from Cave Hill, Barbados. *Quaternary Science Reviews*, *295*, 107783.

Toomey, M., Ashton, A. D., & Perron, J. T. (2013). Profiles of ocean island coral reefs controlled by sea-level history and carbonate accumulation rates. *Geology*, *41*(7), 731-734.

Van Daele, M., van Welden, A., Moernaut, J., Beck, C., Audemard, F., Sanchez, J., ... & De Batist, M. (2011). Reconstruction of Late-Quaternary sea-and lake-level changes in a tectonically active marginal basin using seismic stratigraphy: The Gulf of Cariaco, NE Venezuela. *Marine Geology*, *279*(1-4), 37-51.

Waelbroeck, C., Labeyrie, L., Michel, E., Duplessy, J. C., Mcmanus, J. F., Lambeck, K., ... & Labracherie, M. (2002). Sea-level and deep water temperature changes derived from benthic foraminifera isotopic records. *Quaternary science reviews*, *21*(1-3), 295-305.

Weber, G.E. (1990). Late Pleistocene slip rates on the San Gregorio fault zone at Point Ano Nuevo, San Mateo County, California, *in* Garrison, R.E., et al., eds., *Geology and tectonics of coastal California, San Francisco to Monterey* (volume and guidebook): Bakersfield, California, Pacific Section, American Association of Petroleum Geologists, p. 193–203.

Webster, J. M., Wallace, L. M., Clague, D. A., & Braga, J. C. (2007). Numerical modeling of the growth and drowning of Hawaiian coral reefs during the last two glacial cycles (0–250 kyr). *Geochemistry, Geophysics, Geosystems*, *8*(3).

Geochemistry, Geophysics, Geosystems

Supporting Information for

Reconstructing sea-level and hydroclimates through Bayesian inversion of coastal landforms

G. de Gelder[1,2,3], N. Hedjazian[3], L. Husson[1], T. Bodin[3], A.-M. Pastier[4], Y. Boucharat[1], K. Pedoja[5], T. Solihuddin[2] and S. Y. Cahyarini[2]

[1]ISTerre, IRD, CNRS, Université Grenoble-Alpes, France

[2]Res. Group of Paleoclimate & Paleoenvironment, Res. Centr. for Climate and Atmosphere, Res. Org. of Earth Sciences and Maritime, National Research and Innovation Agency, Bandung, Republic of Indonesia.

[3]CNRS, LGL-TPE, Universite Claude Bernard Lyon1, ENS de Lyon, France

[4]GeoForschungsZentrum, Potsdam, Germany

[5]Université de Caen, Caen, France

Contents of this file

Text S1
Figures S1 to S3

Introduction

This section contains Supplementary text, as well as 3 Supplementary Figures. The text includes further details on the sea-level ranges used in this study. Figure S1 presents inversion results of the Santa Cruz terraces with alternative values for *ipstep*, *σ* and *corrl*, whereas Figure S2 presents inversion results of the Santa Cruz terraces with alternative morphostratigraphic scenarios. Figure S3 presents a map and data from the SE Corinth Rift terraces.

Text S1.

Paleo sea-level ranges

The red boxes in Fig. 1c provide estimates of the likely range of relative sea-level (RSL) variations at far-field locations. The subdivision of boxes is based on the marine isotope stages (MIS) and their sub-stages defined by Railsback et al. (2015); with the exception of MIS 11a, which we split into three sub-stages based on the shape of the sea-level curve of Spratt & Lisiecki (2016) and the proposed two RSL highstands at the Huon Peninsula for that period (de Gelder et al., 2022). Time ranges are based on the sea-level curve of Spratt & Lisiecki (2016), with the exception of MIS 1 and MIS 2, for which we used the time ranges proposed by Kahn et al. (2015) and Clark et al. (2009), respectively.

The RSL datapoints are selected from the database of Hibbert et al, (2016), complemented with data from Murray-Wallace (2002), de Gelder et al. (2022), and Marra et al. (2023). We limited these to data older than 130 ka, and with total elevation uncertainties of less than 35 m (±17.5m). Concerning the data points from the Hibbert et al. (2016) database we applied the same filters as was done in the publication of their compilation, only using U/Th data with calcite <2%, ^{232}Th concentration <2 ppb and $\delta^{234}_{initial}$ of 147 +5/-10‰. The remaining RSL datapoints are from Stirling et al. (2001) and Andersen et al. (2010), for which we used the ±1σ uncertainties in time and elevation from the database (Hibbert et al., 2016). For the age uncertainty on the Murray-Wallace (2002) RSL estimates we used the time ranges of the red boxes as age error margins, and assigned an arbitrary elevation uncertainty of ±5 m. For de Gelder et al. (2022) we used the published time and elevation standard errors, whereas for Marra et al. (2023) we used the time ranges of the red boxes as age error margins, and assigned an elevation uncertainty of ±1 m as proposed in their paper.

In terms of the elevation ranges of the red boxes, for MIS 1 we used the proposed Mid-Holocene range by Kahn et al. (2015). For MIS 2 we used the minimum from Spratt & Lisiecki (2016) and the maximum from Gowan et al. (2022). For MIS 3 we used the minima from Spratt & Lisiecki (2016) and the maximum from Pico et al. (2016). For MIS 4, 5b, 5d, 6a, 8a, 10a and 12a we used the minima and/or maxima from Spratt & Lisiecki (2016) and Batchelor et al. (2019). For MIS 5a and 5c we used the minima from from Spratt & Lisiecki (2016) and the maxima from Creveling et al. (2017). For MIS 5e we used the minimum from Dyer et al. (2021) and the maximum from Kopp et al. (2009) and Dutton et al. (2015). For MIS 6b, 6c, 6d, 6e, 7a, 7c, 7e, 9a, 9e, 11a-1 and 11a-3 we used the minima from Spratt & Lisiecki (2016) and the maxima from the RSL data points. For MIS 7b we used the minimum from Spratt & Lisiecki (2016) and the maximum from the MIS 7a box. For MIS 7d we used the same range as MIS 6e. For MIS 8b we used the minimum from Spratt & Lisiecki (2016) and the maximum from the MIS 8c box. For MIS 8c, 9c, 9d and 12b we used the minimum and maximum from Spratt & Lisiecki (2016). For MIS 9b we used the minimum from Spratt & Lisiecki (2016) and the maximum from the MIS 9a box. For MIS 11a-2 we used the minimum from Spratt & Lisiecki (2016) and the maximum from the MIS 11a-1 box. For MIS 11b we used the minimum from Spratt & Lisiecki (2016) and the maximum from the MIS 11a-3 box. For MIS 11c we used the minima from Murray-Wallace (2002) and Marra (2023) and the maximum from Dutton et al. (2015).

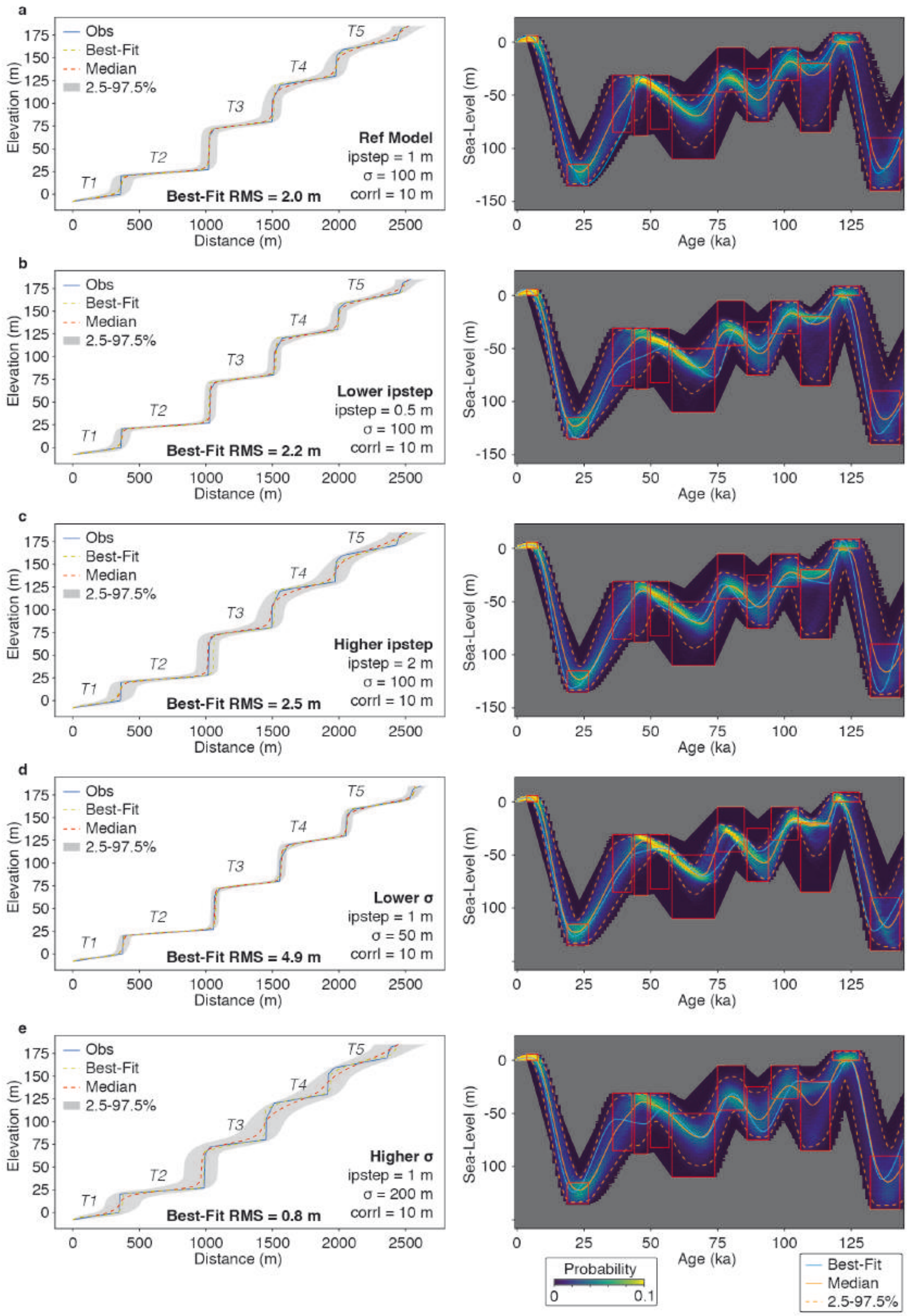
a
b
c
d
e
Obs
Best-Fit
Median
2.5-97.5%
T1
T2
T3
T4
T5
Elevation (m)
Distance (m)
Ref Model
ipstep = 1 m
σ = 100 m
corr = 10 m
Best-Fit RMS = 2.0 m
Lower ipstep
ipstep = 0.5 m
Best-Fit RMS = 2.2 m
Higher ipstep
ipstep = 2 m
Best-Fit RMS = 2.5 m
Lower σ
σ = 50 m
Best-Fit RMS = 4.9 m
Higher σ
σ = 200 m
Best-Fit RMS = 0.8 m
Sea-Level (m)
Age (ka)
Probability
0
0.1

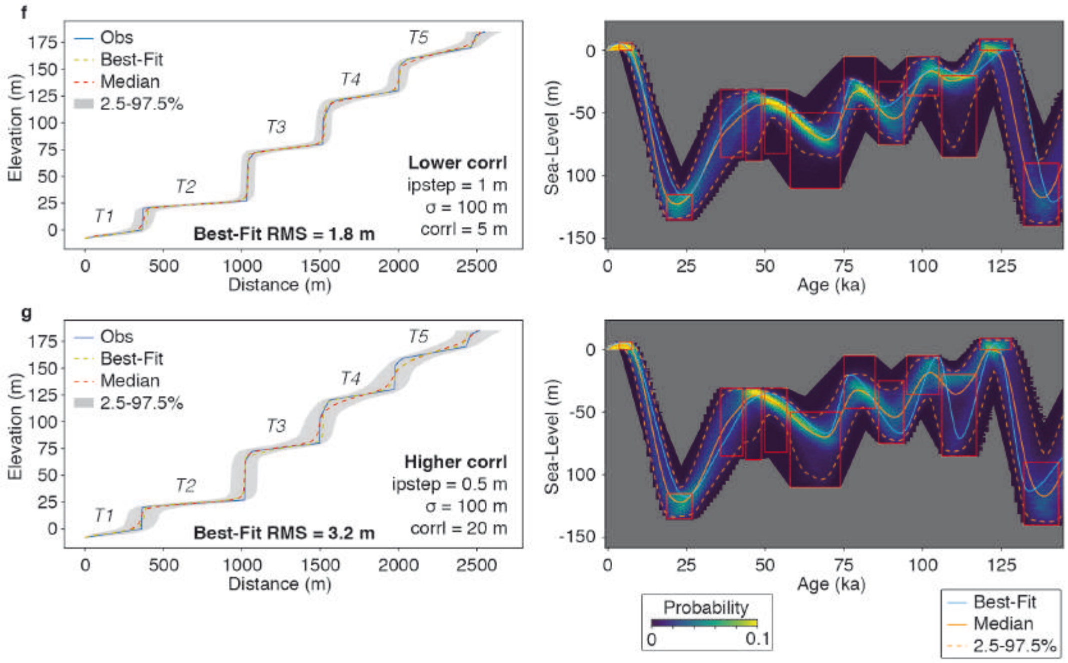

Figure S1. Santa Cruz terrace sequence tests with different inversion parameters. **a)** Same as Fig. 3, for comparison with inversions that use a **b)** lower ipstep, **c)** higher ipstep, **d)** lower σ, **e)** higher σ, **f)** lower corrl and **g)** higher corrl. Note that the ranges for accepted terrace profiles tend to increase or decrease (left side), but the range of sea-level does not change much (right side).

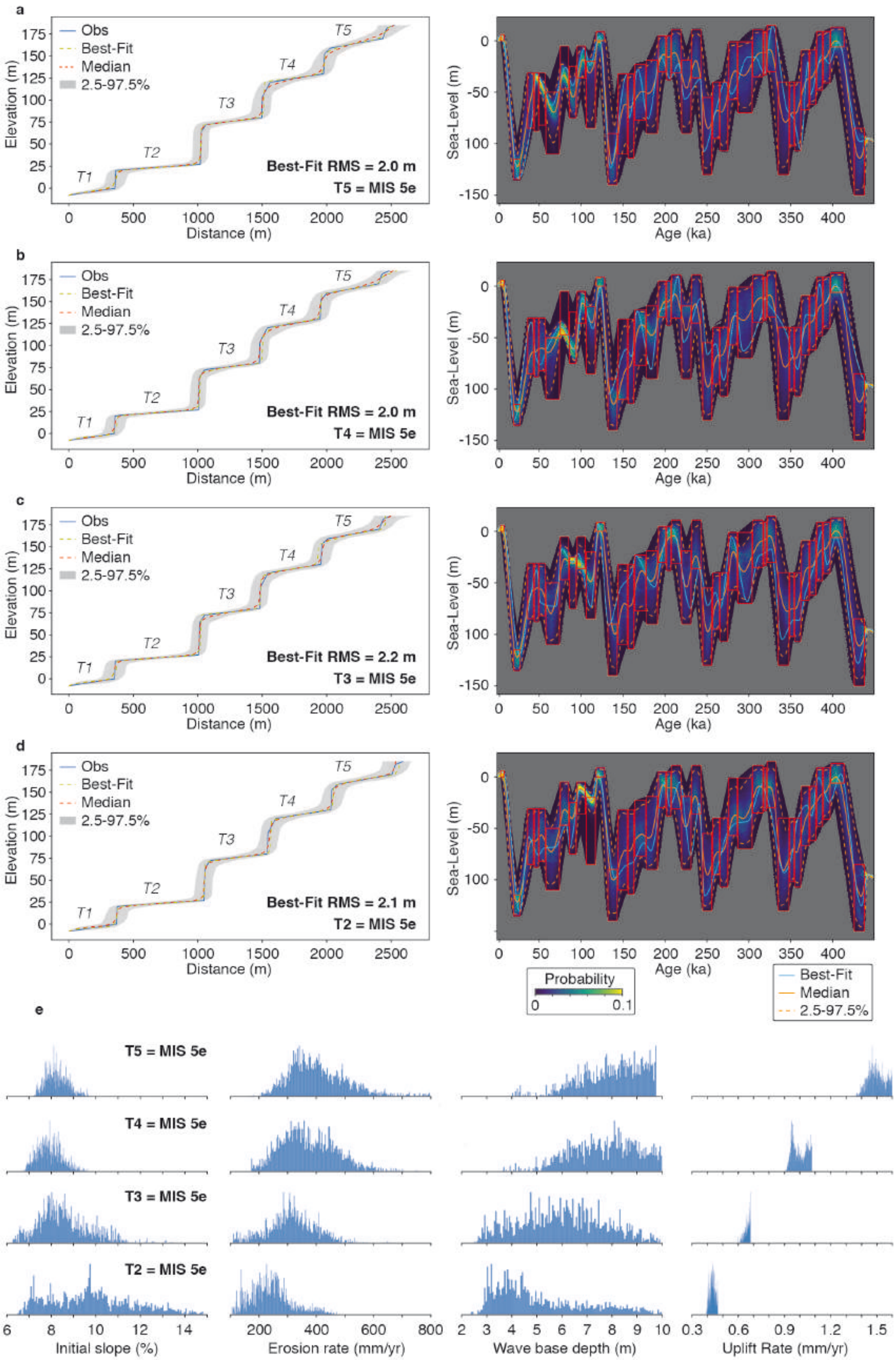

a
Obs
Best-Fit
Median
2.5-97.5%
T1
T2
T3
T4
T5
Best-Fit RMS = 2.0 m
T5 = MIS 5e
Elevation (m)
Distance (m)
Sea-Level (m)
Age (ka)
b
Best-Fit RMS = 2.0 m
T4 = MIS 5e
c
Best-Fit RMS = 2.2 m
T3 = MIS 5e
d
Best-Fit RMS = 2.1 m
T2 = MIS 5e
Probability
0
0.1
Best-Fit
Median
2.5-97.5%
e
T5 = MIS 5e
T4 = MIS 5e
T3 = MIS 5e
T2 = MIS 5e
Initial slope (%)
Erosion rate (mm/yr)
Wave base depth (m)
Uplift Rate (mm/yr)

Figure S2. Santa Cruz terrace sequence tests with different uplift rates. **a)** Same as Fig. 3, for comparison with inversions that use an uplift rate of **b)** 0.9-1.1 mm/yr, **c)** 0.5-0.7 mm/yr, and **d)** 0.3-0.5 mm/yr **e)** Ranges of initial slope, erosion rate, wave base depth and uplift rate that correspond to the four scenarios in **a-d**

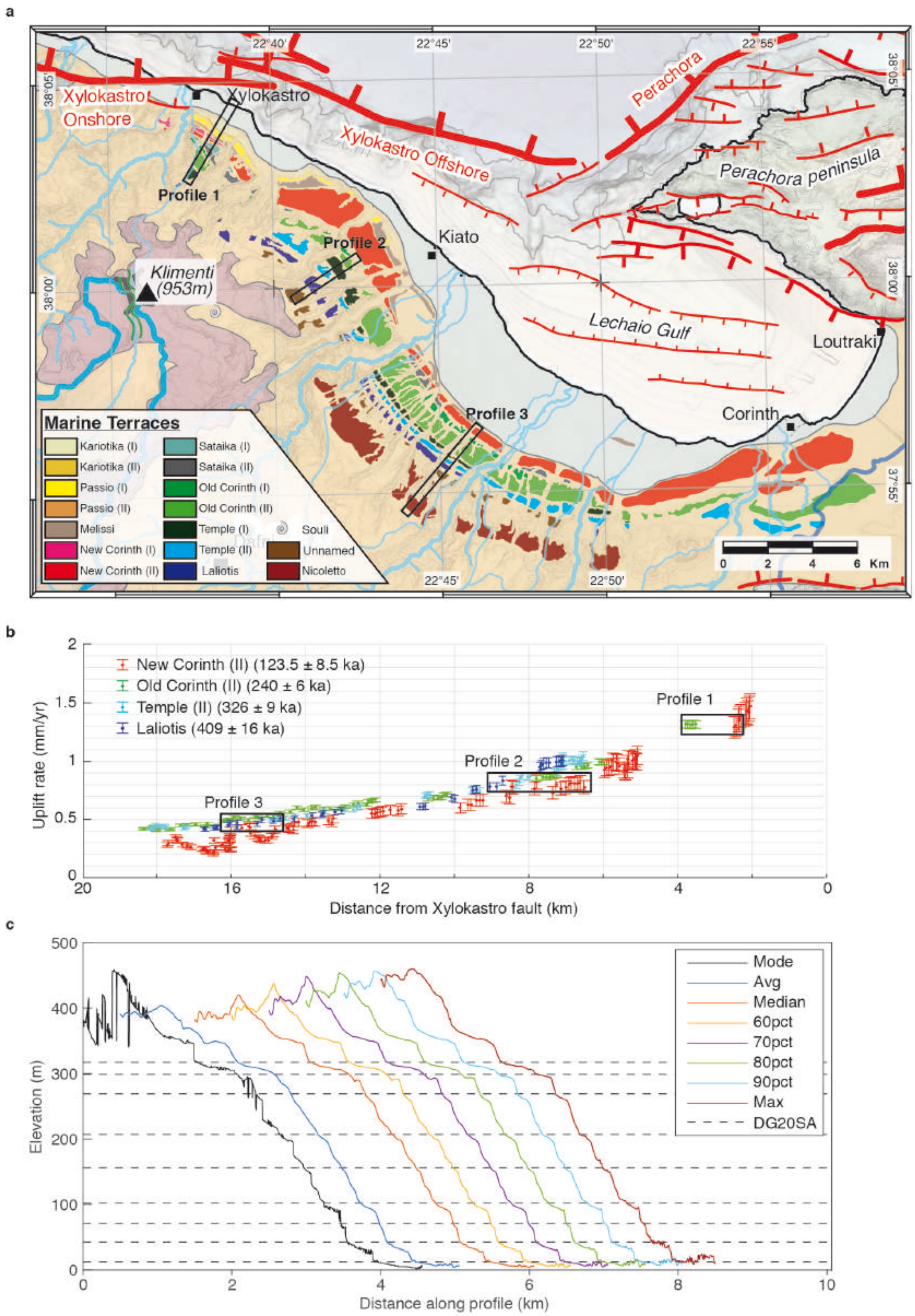

Figure S3. SE Corinth Rift terraces. **a)** Map of the SE Corinth Rift (modified from De Gelder et al., 2019) with locations of the inverted profiles. **b)** Uplift rates as a function of distance from the fault (modified from De Gelder et al., 2019) with locations of the inverted profiles. **c)** Different characterizations of the topography within the profiles of a, compared to the average shoreline angle elevations calculated in De Gelder et al. (2020).